Desalination and Water Treatment
www.deswater.com
doi: 10.1080/19443994.2014.887038

54 (2015) 1594–1603
May

Taylor & Francis
Taylor & Francis Group

Fluoride removal from drinking water by zirconium-impregnated fibrous protein

Hui Deng[a,*], Xili Yu[b]

[a]*Department of Chemistry, Chemical and Environment, Liaoning Shihua University, Fushun 113001, China*
Tel. +86 2456860759; Fax: +86 2456860008; email: dengchong060920@gmail.com
[b]*School of Chemistry Chemical and Biological Engineering, University of Donghua, Shanghai 021, China*

Received 6 August 2013; Accepted 20 January 2014

ABSTRACT

Zirconium-impregnated fibrous protein (ZrFP) adsorbent was synthesized by recovering fibrous protein (FP) with zirconium sulfate with immobilization reaction at pH 3.0–4.0. The adsorbent was characterized, and its performance for fluoride removal in drinking water was evaluated. Zirconium was well dispersed and impregnated on FP surface from SEM photos. Fourier transform infrared showed that the hydroxyl group of hydrous metal oxide (Zr-OH) appeared at 1,130 cm^{-1} after impregnation. ZrFP showed an alkaline surface charge property and exhibited the best efficiency at pH 5.0 with a fluoride sorption capacity of 12.6 mg/g at equilibrium concentration of 1.0 mg/L. Fluoride sorption kinetics was well described by the pseudo-second-order model, and sorption equilibrium was suitable to the Langmuir isotherm equation. It was found that the release of Zr(IV) in residual solution was below 0.3 mg/L, and column sorption experiment indicated the drinking water quality was improved by fluoride adsorption.

Keywords: Zirconium-impregnated fibrous protein (ZrFP); Fluoride adsorption; Drinking water

1. Introduction

Fluoride in drinking water is one of major sources for fluoride exposure to general population. For example, in the south of Brazil, artesian-well waters from rock rich in calcium and silicon contain 5–20 mg/L of fluoride [1]. Also in some natural water systems over large areas in Asia, America and Europe, the fluoride concentration ranges from 0.01 to 3 mg/L in fresh water and 1–35 mg/L in ground water [2]. According to the World Health Organization, the optimum fluoride level in drinking water for general good health is between 0.5 and 1.5 mg/L [3]. Excessive intake of fluoride leads to dental and skeletal fluorosis [4,5]. High levels of fluoride concentration in groundwater are affecting millions of people in many countries such as China, India, Sri Lanka, Ghana, Ivory Coast, Senegal, Algeria, Kenya, Uganda, Tanzania, Ethiopia, Mexico and Argentina [6].

Different techniques have been developed for fluoride removal such as chemical precipitation, electrolysis, reverse osmosis, nanofiltration, ion exchange and adsorption [7–9]. Adsorption is one of the most commonly used way for defluoridation due to its ease of operation and cost-effectiveness. Several adsorbents have been used such as activated carbon [10], metal oxides [11] and some low-cost materials, both natural

*Corresponding author.

and synthetic [12], as well as biomaterials [13]. Specially, activated alumina [14] is always most widely used for defluoridation of drinking water. However, frequent regeneration with aluminum sulfate is needed because of its low adsorption capacity at neutral pH [15], resulting in increased difficulty in operation.

It recent year, Zr(IV) oxides have been reported to have high affinity to fluoride and arsenic [16], because tetravalent zirconium in its hydrated form can generate tetranuclear ions as well as octanuclear species, which have abundant hydroxyl ions and water molecules to take part in ligand substitution with arsenic and fluoride anions [17]. Thus, various Zr(IV)-loaded adsorbents have been developed for the removal of fluoride from aqueous solution [16–21]. Zirconium(IV)-ethylenediamine (ZrEDA) hybrid material was prepared following an environmental friendly sol–gel method, and it was found that the extent of fluoride removal was more than 99%, and fluoride adsorption equilibrium was attained in a 14-min time period [20]. Zirconium-impregnated cashew nut shell carbon (ZICNSC) was studied to assess its capacity of fluoride adsorption from aqueous solutions, and 80.33% salt rejection has been identified in 3 mg/L of 100 mL fluoride using 1.5-mg dosage of adsorbent [21].

Zirconium is generally non-toxic as an element or in compound, and the oral toxicity is reported to be quite low [22]. Activated charcoals impregnated with zirconium metal ions have an increase in fluoride adsorption capacity by 3–5 times to that of plain activated charcoal for drinking water [23]. Fibrous protein (FP) is a kind of structure protein, usually formed and prepared from skin, bone and connective tissue of animals. Based on the results available from the literature and previous study [24], the aim of this study was to determine the adsorption properties of zirconium-impregnated fibrous protein (ZrFP) for treating effluents of lower fluoride concentrations of 2–50 mg/L [25]. Sorption experiments including pH effect, sorption kinetics and sorption isotherm were investigated in details. The column study was conducted to evaluate the suitability of ZrFP for natural drinking water.

2. Materials and methods

2.1. Materials

The FP (a common commercial product) was provided by China Academy of Forest, Nanjin, China. All chemicals were of reagent grade.

2.2. Synthesis of ZrFP

ZrFP was synthesized by reaction of zirconium sulfates and FP. The initial pH value of reaction solution was maintained at 1.5–2.0 by 1 M H_2SO_4, thus the FP was added according to a stoichiometric ratio 1.64 of FP to Zr(IV). At the same time, the reaction temperature was increased to 40˚C, and solution was modified at pH 3.0–4.0 by gradual addition of sodium bicarbonate. Constantly stirring for 6–7 h, the ZrFP adsorbent formed was rinsed with distilled water until no residual Zr(IV) metal ion was detected by inductively coupled plasma-atomic emission spectroscopy (ICP-AES, Perkin–Elmer Optima 2100DV, Germany) and dried below 60˚C.

2.3. Characterization

The Zr(IV) content was obtained by measuring the residual Zr(IV) amount in loading reaction solution using ICP-AES (ICP, Perkin–Elmer Optima 2100DV, Germany). The specific areas of ZrFP were determined by a surface area and porosity analyzer (Tristar3000, Micromeritics, US). The surface morphology of the adsorbent was observed by scanning electron microscope (SEM, JSM-5900LV). Fourier transform infrared (FTIR) spectra of ZrFP adsorbent was recorded on Perkin–Elmer (USA) system 2000 spectrophotometer with a resolution of 2 cm^{-1}. The heat denaturation temperatures of ZrFP were determined by differential scanning calorimetry (DSC, PC 200DSC, NETZSH Company, Germany) with a heating rate 5˚C/min. The pH of zero point charge measurement (pH_{zpc}) was detected by the solid addition method [26]. Accordingly, a series of well stoppered 125-mL polyethylene bottle containing 40 mL of desired electrolyte solution, different volumes of either 0.1 M HCl or 0.1 M NaOH solution were added in such a way so as to obtain wide ranging pH values (pH 2–10). The total volume of solution in each bottle was made up to 50 mL by the relevant electrolyte solution. After 2 h of equilibration, the pH values were noted. These were designated as initial pH values or pHi. A known amount of solid oxide/mixture of oxides was added in each bottle which was then flushed with nitrogen gas for 3–5 min and then stopped securely. After 72 h of equilibration at 300 K with intermittent shaking, the pH values of the supernatant liquid in each bottle was noted and designated as final pH or pHf. The difference between pHi and pHf (ΔpH) was plotted against pHi. The resultant curve intersects ΔpH = 0 at a certain value of pHi. This means that at this pH, the oxides or mixture of oxides do not induce the release of

either H^+ or OH^- ion in solution, i.e. the surface does not undergo or acquire any charge through acid–base dissociation, a condition for pH_{pzc}. And other physical properties were determined by common methods.

2.4. Sorption experiments

Fluoride adsorption on ZrFP was performed using natural drinking water. Batch experiments were conducted in 250-mL flasks containing 100 mL fluoride drinking solution. 0.1 g ZrFP was dispersed in each flask and shaken at 120 rpm in a thermostatic shaker at 25°C for 24 h for equilibrium. Thereafter, the adsorbent particles were separated immediately by filtration. The filtrate pH was measured, and the fluoride concentration was analyzed by ion selective electrode method. The total adsorbed fluoride on ZrFP surface was calculated from the difference between the initial and residual concentration of fluoride in solution. The chemical stability of the inorganic metal content of ZrFP was studied by measuring Zr(IV) release in solution, and Zr(IV) concentration was determined using ICP-AES (ICP, Perkin–Elmer Optima 2100DV, Germany).

The effect of equilibrium pH on fluoride adsorption was investigated by adjusting the pH of solution to 2.0–12.0 under an initial F^- concentration of 9.5 mg/L. A kinetics study was carried out at natural pH at different time intervals with initial F^- concentration of 9.5 and 19 mg/L. The sorption isotherm experiments at natural pH were studied by varying initial concentration of anions from 2 to 50 mg/L in 283 K, 298 K and 313 K.

Continuous fixed bed adsorption was carried out with perspex column (internal diameter 0.9 cm, length 50 cm). The mass of ZrFP required was 0.1 g/cm of the column bed with packed bed density 0.17 g/cm^3. The inlet flow rate was 0.4 mL/min controlled by a flow controller, and the initial pH of the feed fluoride solution was about 6.8. Samples in fixed bed runs were collected at regular intervals of time for measurement of residual fluoride. Common ions (Cl^-, HCO_3^-, SO_4^{2-}, NO_3^-, Na^+, K^+, Ca^{2+} and Mg^{2+}) in drinking water were detected using ICP-AES in influent and effluent respectively to investigate their effects on fluoride adsorption by ZrFP.

3. Results and discussion

3.1. Characterization of ZrFP

The fiber was just like powders with 0.1–0.25 mm diameter and not so long as usual fibers. As can been

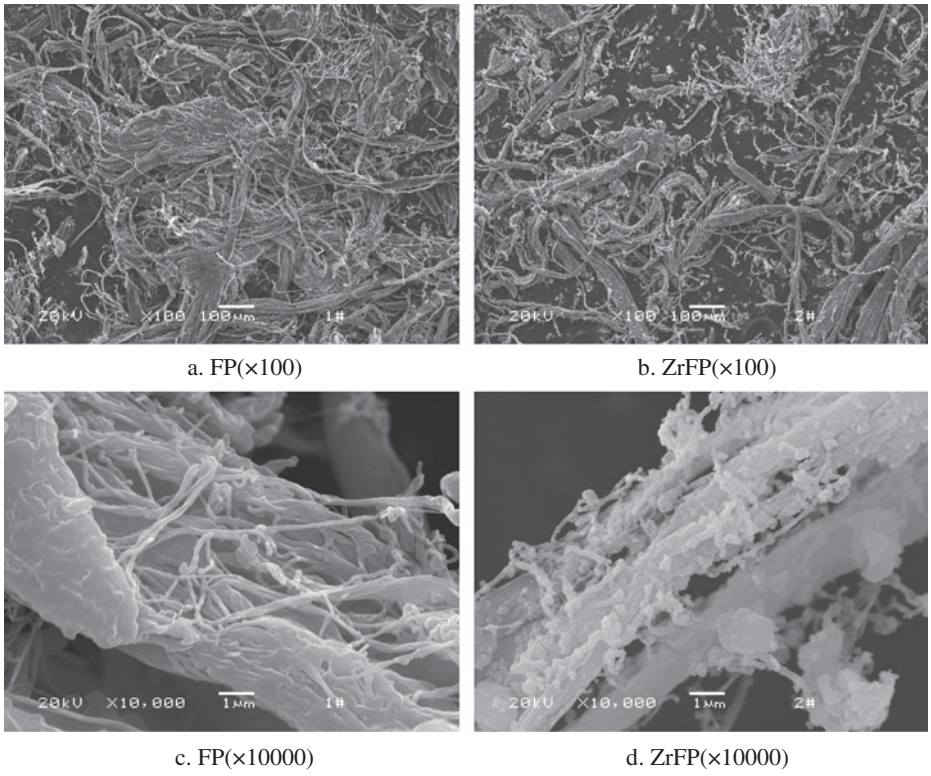

a. FP(×100) b. ZrFP(×100)

c. FP(×10000) d. ZrFP(×10000)

Fig. 1. SEM images of FP (a,c) and ZrFP (b,d).

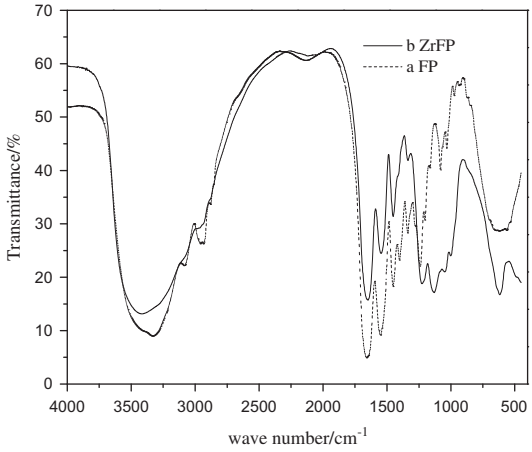

Fig. 2. FTIR spectra of (a) raw material (FP) and (b) prepared adsorbent (ZrFP).

seen from (Fig. 1(a) and (b)) were at lower magnification, while (Fig. 1(c) and (d)) were at higher magnification. FP surface (Fig. 1(c)) was smooth, and no prominent coating was observed, but in (Fig. 1(d)), it was clearly visible that the ZrFP fibers were covered by large quantities of fine grains, maybe prone to the formation of uniform Zr(IV) complexes on FP surface during the impregnation procedure. The hydroxide formation onto FP surface was confirmed through FTIR spectra of ZrFP vs. FP in (Fig. 2). Great band at 3,330–3,600 cm^{-1} assigned to the stretching vibration of –OH on carboxyl, and the strong band at around 1,130 cm^{-1} of ZrFP (Fig. 2(b)) attributed to the Zr-OH bond stretching [27], unable to be observed in FTIR spectra of FP in (Fig. 2(a)). These intensified bands for –OH group indicated that Zr(IV) has been bonded onto the surface of FP; furthermore, the metal hydroxyl group of ZrFP would play an important role in fluoride adsorption [27].

The physical properties of FP and ZrFP were listed in Table 1. The specific area of ZrFP adsorbent was much smaller than some porous adsorbents such as activated carbon (1,044 m^2/g [28]), which implied that the mass transfer of fluoride adsorption process may mainly attribute to chemical reaction between Zr(IV) and fluoride rather than physical adsorption depending on high specific area of adsorbent. Simultaneously, modification of FP by Zr(IV) significantly shifted the pH_{pzc} from acidic to alkaline range, pH_{pzc} 5.4–5.6 to pH_{pzc} 9.0–9.35. Thus, the potential of the ZrFP surface was positive in solution when pH below 9.35, thus ZrFP was expected to exert better fluoride adsorption performance than FP since the positive surface charge range was widened, and surface electrostatic interaction between adsorbent and fluoride in the solution was enhanced.

4. Fluoride removal

4.1. Effect of pH

The pH of the medium was an important parameter that significantly affected the extent of fluoride adsorption. Fig. 3 showed the effect of pH on the fluoride uptake using ZrFP. Optimal fluoride removal by ZrFP occurred in the pH range of 3–7. The maximum fluoride adsorption capacity was found to be 8.7 mg/g at pH 5.0 corresponding to a fluoride removal yield of 92%. This was consistent with the result obtained in the pH range of 2.0–7.0 by Zr(IV)-ethlenediamine [20] and the optimum pH range of 3.5–7.5 using zirconium-modified-Na-attapulgite adsorbent [17]. The ion-electric point (IEP) of the adsorbent material was 9.0–9.35 according to Table 1. The maximum adsorption occurred at $pH < pH_{pzc}$, since at $pH < pH_{pzc.}$ The adsorbent was positive and attracted the negative fluoride ions. The quick reduction in fluoride adsorbed took place in the alkaline pH range due to competition of hydroxyl ions with fluoride for adsorption sites [29] and electrostatic

Table 1
Physical properties of o-fibrous protein and Zr-fibrous protein

Property items	Limits	
	o-fibrous protein	Zr-fibrous protein
Particle size	11.71–16.16 nm	15.61–16.84 nm
Bulk density (dry)	0.051–0.053 g/cm^3	0.0579–0.0621 g/cm^3
Carbon surface area	2.11–2.15 m^2/g	3.57–3.65 m^2/g
Pore volume	0.0192–0.0196 cm^3/g	0.0064–0.0075 cm^3/g
Moisture	1.83–2.22 gH_2O/g	3.14–3.50 gH_2O/g
Metal ion content	–	0.5200–0.5800 g/g
Denaturation temperature	331–333 K	371–373 K
pH_{pzc}	5.4–5.6	9.0–9.35

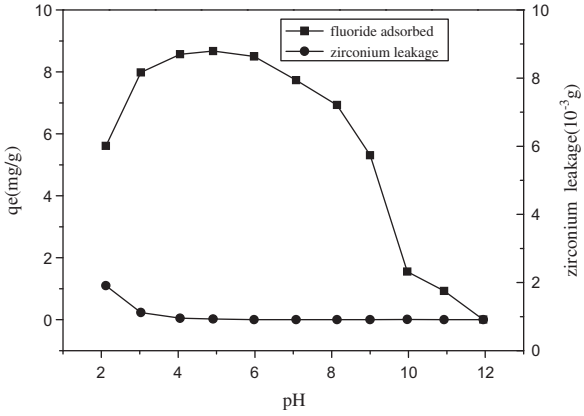

Fig. 3. Effect of pH on fluoride adsorption by ZrFP (1 g/L adsorbent, initial fluoride concentration was 9.5 mg/L, 298 K).

repulsion of fluoride ion to the negatively charged surface [25] of ZrFP.

In addition, as shown in Fig. 3, the dissolution of Zr (IV) ions was determined, and nearly no zirconium ions (<0.3 mg/L) were leaked out during the whole pH adsorption range, in favor of fluoride removal in drinking water. The origin pH of fluoride drinking water was 6.53–6.83 and located in the optimum adsorption pH range; therefore, it was unnecessary to adjust solution pH in the following adsorption experiments.

The pH recorded before and after adsorption experiment was shown in Fig. 4, the decrease in solution pH during adsorption was advantageous for defluoridation, and similar observation was noted previously for different type of adsorbents [17,20,25,30]. Zhang et al. [17] suggested that

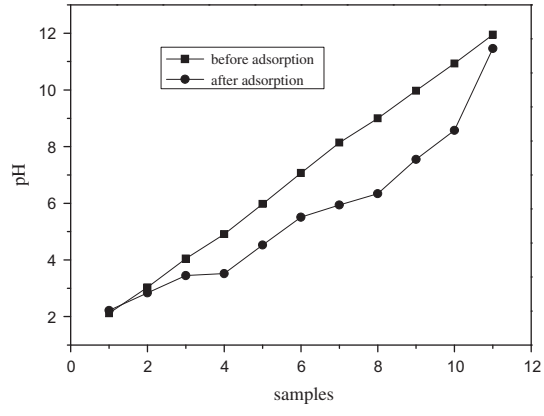

Fig. 4. The pH of fluoride solution before and after adsorption (1 g/L adsorbent, initial fluoride concentration was 9.5 mg/L, 298 K).

mechanism of fluoride adsorption by Zr-A was described as:

$$\equiv Zr(OH)_2 \bullet nH_2O + F^-_{aq} + Na^+_{(aq)} \Longleftrightarrow \equiv Zr(OH)_2 \bullet (n-1)H_2OOH^-Na^+F^-_{(solid)} + H^+$$

and a drop of pH of the equilibrated solution when initial solution pH > 7.50 aroused from intervention of Na^+ ion. Swain et al. [20] inferred MZrP acted as a cation exchanger and adsorbed Na^+ ion present in solution, thereby releasing protons responsible for overall decrease in final pH of the medium when pH > pH_{pzc}. Nigamananda Das et al. [25] believed that this decrease in equilibrium pH in defluoridation by TRB was a consequence of two-step ligand exchange mechanism operated during adsorption of fluoride:

$$\equiv SOH_{(s)} + H^+ + F^-_{(aq)} \Longleftrightarrow \equiv SF_{(s)} + H_2O$$

Eric Tchomgui-Kamga et al. [30] maintained that the observed decrease in equilibrium solution pH indicated that the fluoride adsorption mechanism using AlFe650/C was dominated by:

$$M - Cl_{(s)} + H_2O \rightarrow M - OH_{(s)} + H^+_{(aq)} + Cl^-_{aq}$$

ZrFP was a little different from the above materials that all of the solution pH have fallen whether initial pH was lower or higher than the pH_{pzc}. At a lower pH (pH < pH_{pzc}), it was interfered that the zirconium hydrous oxides could be protonated, and the sorption may take place as ion exchange Scheme (1) [24]. However, the adsorption of fluoride is not only the result of ion exchange but also the result of the nucleophilic SN2-i replacement of OH-groups combined with Zr atoms by fluoride with the formation of intermediate six-numbered complex as Scheme (2) [31].

$$Zr - OH^+_2 + F^- \Longleftrightarrow ZrF + H_2O \quad (1)$$

$$Zr - OH^+_2 + F^- \Longleftrightarrow Zr - OH - F^- + H^+ \Longleftrightarrow ZrOF + 2H^+ \quad (2)$$

At a higher pH (pH > pH_{pzc}), the surface of the adsorbent is negative, therefore, fluoride adsorption capacity reduced due to the repulsion of like charges that existed between the solute in solution (F^-) and the solid surface. Simultaneously, the zirconium hydrous oxides could be deprotonated in the following Scheme (3) [32]:

$$Zr - OH + OH^- \Longleftrightarrow Zr - O^- + H_2O \quad (3)$$

4.2. Adsorption kinetics

Adsorption kinetics was one of the most important characteristics which represented the adsorption efficiency. The sorption kinetics of fluoride at different initial concentrations on ZrFP adsorbent was shown in Fig. 5. The adsorption was fast in first 2–30 min depending on initial fluoride concentration, before the curve became more gradual until equilibrium was reached. It took approximately 6 h for initial fluoride 9.5 mg/L adsorption on ZrFP to reach the pseudo-equilibrium and 8 h for 19 mg/L.

The analysis of kinetics adsorption data was based on the pseudo-first-order model, the pseudo-second-order model and the intra-particle diffusion model [33].

The pseudo-first-order model:

$$\log(q_e - q_t) = \log q_e - k_1 t/2.303 \quad (4)$$

The pseudo-second-order model:

$$t/q_t = 1/k_2 q_e^2 + t/q_e \quad (5)$$

The intra-particle diffusion model:

$$q_t = k_i t^{0.5} \quad (6)$$

where q_e was the equilibrium adsorption capacity (mg/g); q_t was the adsorption capacity at the time of t (min); and k_1, k_2 and k_i were rate constant of the pseudo-first-order model, pseudo-second-order model and intra-particle diffusion model, respectively. Fig. 6 illustrated the kinetics of fluoride adsorption on ZrFP, and the adsorption kinetics model parameters were given in Table 2. As shown in Table 2, it was evident that fluoride adsorption on ZrFP was suitable for the pseudo-second-order model with greater correlation coefficients (R^2) values (0.9970–0.9975) than other two models. The pseudo-second-order equation was often adopted to describe the chemisorption assumption that rate-limiting step may be chemical sorption or chemical bonding involving valence forces through sharing or exchange electrons between adsorbent and adsorbate [34] and has been widely applied to the adsorption of pollutants from aqueous solution in recent years. Furthermore, this model assumed that the adsorption followed the Langmuir equation [35].

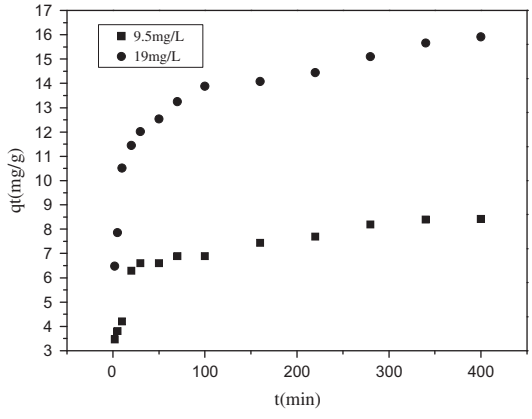

Fig. 5. Adsorption kinetics of fluoride on ZrFP (1 g/L adsorbent, initial pH of fluoride solution was 6.54, initial fluoride concentration was 9.5 and 19 mg/L, 298 K).

4.3. Equilibrium adsorption isotherm

The fluoride sorption isotherm on the ZrFP at 283 K, 298 K and 313 K was shown in Fig. 7. It can be seen that the sorption capacity at equilibrium (q_e) gradually increased with increasing equilibrium fluoride concentrations.

Analysis of isotherm data was very important for predicting the adsorption capacity of adsorbent, which was one of the main parameters required for the design of an adsorption system. Langmuir and Freundlich equations were adopted to evaluate various sorption parameters.

Langmuir model assumed that adsorption forces were similar to the forces in chemical interactions and that valid for monolayer sorption onto a surface was described as [36]:

$$q_e = bQ_0C_e/(1 + bC_e) \quad (7)$$

where C_e was equilibrium concentration (mg/L), q_e was the amount adsorbed under equilibrium (mg/g), Q_0 was the theoretical maximum adsorption capacity, and b (L/mg) was a Langmuir constant, indicating the affinity of the F^- toward the adsorbent. The values of Langmuir parameters, Q_0 and b, were calculated from the slop and intercept of the linear plots of $1/q_e$ vs. $1/C_e$ presented in Table 3.

The Freundlich adsorption isotherm was based on the multilayer adsorption of an adsorbate onto the heterogeneous adsorbent surface and could be expressed as [37]:

$$q_e = k_F C_e^{\frac{1}{n}} \quad (8)$$

Table 2
Adsorption kinetics parameters of ZrFP to fluoride (9.5 and 19.0 mg/L)

Dynamic equations	Fluoride concentration	Dynamic parameters	Correlations coefficient R^2
Pseudo-first-order equation	9.5	$k_1 \times 10^3 = 3.915$	0.8649
$\log (q_e - q_t) = \log q_e - k_1 t/2.303$	19	$k_1 \times 10^3 = 2.764$	0.8298
Pseudo-second-order equation	9.5	$k_2 \times 10^3 = 9.243$	0.9970
$t/q_t = 1/k_2 q_e^2 + t/q_e$	19	$k_2 \times 10^3 = 6.068$	0.9975
Particle diffusion equation	9.5	$k_T = 0.2409$	0.8187
$q_t = k_T t^{1/2}$	19	$k_T = 1.3389$	0.9669

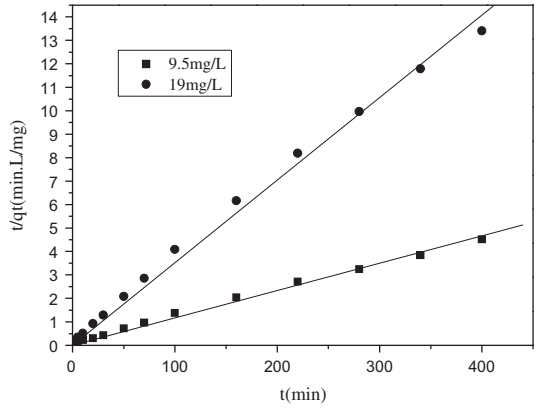

Fig. 6. Pseudo-second-order rate model fitting of adsorption kinetics data (1 g/Lv adsorbent, initial pH of fluoride solution was 6.54, initial fluoride concentrations were 9.5 and 19 mg/L, 298 K).

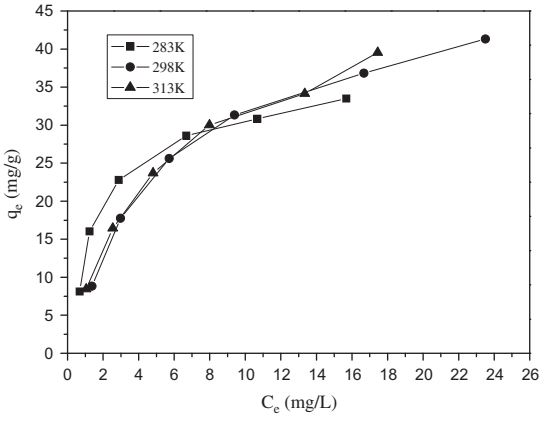

Fig. 7. Adsorption of fluoride on ZrFP at 283 K, 298 K and 313 K (1 g/L adsorbent, initial pH of fluoride solution is 6.54).

where k_F and $1/n$ was Freundlich constants, related to adsorption capacity and adsorption intensity (heterogeneity factor), respectively. The values of k_F and $1/n$ were obtained from the slope and intercept of the liner Freundlich plot of log q_e vs. log C_e. The values of $1/n$ lying between 0 and 1 confirmed the favorable conditions for adsorption, as listed in Table 3.

It can be seen that the Langmuir model fitted the experimental data better than Freundlich model according to the high-correlation coefficients R^2. The maximum sorption capacity Q_0 could attain 50 mg/g at 313 K in terms of the Langmuir model, but the sorption capacity at low fluoride concentration was extremely important for actual drinking water treatment since the final fluoride in residual solution must be below 1 mg/L. The sorption capacity of ZrFP adsorbent was 12.6 mg/g at the equilibrium concentration of 1 mg/L, higher than that of activated alumina, ferric hydroxide, iron–aluminum-mixed oxide and Fe–Al–Ce trimetal oxide [38], as shown in Table 4.

To evaluate the thermodynamic feasibility and further analyze the nature of the adsorption process, three basic thermodynamic parameters, standard free energy (ΔG°), standard enthalpy change (ΔH°) and standard entropy change (ΔS°) were calculated. The negative values of ΔG°(−6.486 kJ mol^{-1} at 283 K, −5.064 kJ mol^{-1}at 298 K and −4.314 kJ mol^{-1}at 313 K) indicated that the sorption of fluoride on the adsorbent was spontaneous under the experimental conditions. ΔS° and ΔH° were calculated to be 0.2492 kJ (mol K)$^{-1}$ and 2.244 kJ mol^{-1}, respectively. The positive value of the ΔH° indicated that the fluoride sorption process on the adsorbent was definitely endothermic in nature, while the positive value of the ΔS° suggested that the fluoride adsorption on the adsorbent surface occurred possibly due to the release of lot of molecular water at the solid–liquid interface during the sorption process [39].

4.4. Column adsorption

The characteristic shape and position of the breakthrough curve (BTC) on the volume axis for a fixed laterite bed 20 cm long were presented in

Table 3
Langmuir parameters of fluoride and phosphate adsorbed on ZrFP

	Langmuir model			Freundlich model		
Temperature (K)	b (L/mg)	q_m (mg/g)	R^2	k_F	n	R^2
283	0.0655	43.10	0.9708	6.189	1.6310	0.8973
298	0.1295	47.62	0.9929	11.24	1.862	0.9219
313	0.1905	50.00	0.9936	9.263	1.882	0.9725

Table 4
Comparison of adsorption capacity of F^- on different adsorbent

Adsorbent	Adsorption capacity (mg/g)	Equilibrium concentration (mg/L)	pH	Reference
Cellulose@hydroxyapatite (HA) nanocomposites	3.17	1	4.0	[3]
Zirconium-modified-Na-attapulgite (Zr-A)	7.47	1	4.13	[17]
Zirconium(IV)-ethylenediamine (ZrEDA)	32.25	1	7.0	[20]
Zirconium-impregnated cashew (ZICNSC)	4.00	1	3.0	[21]
Activated carbon	0.075	1	7.0	[38]
Activated alumina	0.96	1	7.0	[38]
Ferric hydroxide	3	1	6.0–7.0	[38]
Fe–Al–Ce trimetal oxide	12.2	1	7.0	[38]
Iron–aluminum-mixed oxide	12	1.5	6.9	[38]
Titanium dioxide (TiO_2)	0.642	1	2–5	[40]
Amine functionalized co-polymeric resins	4.20	1	3.0	[41]
Fe(III)–Zr(IV) binary mixed oxide	0.319	1	6.0	[42]
Sulfate-doped Fe_3O_4/Al_2O_3 nanoparticles	13.6	1	7.0	[43]
Protonated cross-linked chitosan particles (PCP)	0.662	1	7.0	[44]
Zr(IV)-impregnated dithiocarbamate-modified chitosan beads (Zr-DMCB)	1.446	1	7.0	[45]
Hydrous zirconium oxide	28.9	1	4.0	[46]
Zirconium hydroxide-modified red mud porous materials (Zr-modified RMPMs)	0.2625	1	3–4	[47]
Zr–Mn composite material	1.77	1	7.0	[48]

Fig. 8. Approximately 291 and 786 BVs corresponding to 20 mg/L and 2.5 mg/L fluoride concentration, respectively, in influent were treated before F^- in the effluent reached 1.0 mg/L. As the feed fluoride concentration increased, the breakthrough time decreased. A sharp BTC was obtained for high fluoride concentration, while the BTC corresponding to low fluoride concentration flattened. Some coexisting ions (Cl^-, HCO_3^-, SO_4^{2-}, NO_3^-, Na^+, K^+, Ca^{2+} and Mg^{2+}) in inlet and outlet at 2.5 mg/L initial fluoride concentration were detected and presented, respectively, in Table 5. The effluent pH dropped to 4.46, consistent with the result in batch experiments. The decrease in Ca^{2+} and Mg^{2+} among coexisting cations revealed that the level of alkalinity and hardness in drinking water could be lowered through fluoride sorption by ZrFP adsorbent. The adsorption

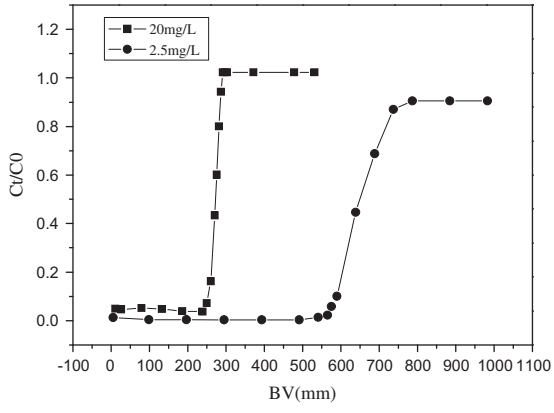

Fig. 8. The BTC at different initial fluoride concentration (1.0 g adsorbent, initial pH of fluoride solution was 6.86, 0.4 mL/min flow rate, 9.5 cm column length, 298 K).

Table 5
The concentration of ions and anions in influent and effluent solution (initial F^- 2.5 mg/L)

Items (mg/L)	pH	Ca^{2+}	Mg^{2+}	Na^+	K^+	NO_3^-	SO_4^{2-}	HCO_3^-	Cl^-
Influent	6.86	66.84	37.8	237.5	91.9	29.28	451.48	387.2	324.3
Effluent	4.46	24.23	13.98	235.3	90.13	27.23	450.3	257.06	291.9

reduction in Cl^- and HCO_3^- was attributed to competition with fluoride for active sorption sites on ZrFP surface. Cl^- has proved to be involved in ion exchange with F^- during fluoride sorption process [21], and HCO_3^- has been reported to exert some negative effect on fluoride adsorption [23]. Similar improvement of water quality parameters has been reported in defluoridation of ZICNSC by Alagumuthu and Rajan [21], where the sample is collected from a nearby fluoride-endemic villages.

5. Conclusion

ZrFP has shown a good efficiency in fluoride removal for drinking water with little Zr(IV) discharge in sorption process. This adsorbent synthesized was alkaline surfaced with $pH_{zpc} < 9.35$. Zirconium ion particles on the surface of FP were shown in SEM images, and the hydroxyl groups on the adsorbent surface were observed by FTIR. An optimum fluoride uptake of ZrFP was obtained at a relatively wide pH range 3.0–7.0. Fluoride sorption on adsorbent was rapid during the first 30 min, and thereafter, it slowly reached pseudo-equilibrium in 6 h for 9.5 mg/L fluoride solution. The adsorption isotherm was better fitted by the Langmuir model. The adsorbent had high sorption capacity up to 12.6 mg F^-/g at equilibrium fluoride concentration of 1 mg/L, much higher than that of some conventional adsorbents. Column tests suggested that ZrFP adsorbent has a promising application in the defluoridation of drinking water.

References

[1] M. Zeni, R. Riveros, K. Melo, R. Primieri, S. Lorenzini, Study on fluoride reduction in artesian well—water from electrodialysis process, Desalination 185 (2005) 241–244.
[2] S.S. Tripathy, J.L. Bersillon, K. Gopal, Removal of fluoride from drinking water by adsorption onto alum-impregnated activated alumina, Sep. Purif. Technol. 50 (2006) 310–317.
[3] X.L. Yu, S.R. Tong, M.F. Ge, J.C. Zuo, Removal of fluoride from drinking water by cellulose@hydroxyapatite nanocomposites, Carbohydr. Polym. 92 (2013) 269–275.
[4] R.C. Meenakshi, R.C. Maheshwari, Fluoride in drinking water and its removal, J. Hazard. Mater. 137 (2006) 456–463.
[5] F. Shen, X. Chen, P. Gao, G. Chen, Electrochemical removal of fluoride ions from industrial wastewater, Chem. Eng. Sci. 58 (2003) 987–993.
[6] K. Babaeivelni, A.P. Khodadoust, Adsorption of fluoride onto crystalline titanium dioxide: Effect of pH, ionic strength, and co-existing ions, J. Colloid Interface Sci. 394 (2013) 419–427.
[7] M. Tahaikt, A.A. Ait Haddou, R. El Habbani, Comparison of the performances of three commercial membranes in fluoride removal by nanofiltration, Continuous operations, Desalination 225 (2008) 209–219.
[8] E. Kumar, A. Bhatnagar, M. Ji, W. Jung, S.H. Lee, S.J. Kim, G. Lee, H. Song, J.Y. Choi, J.S. Yang, B.H. Jeon, Defluoridation from aqueous solutions by granular ferric hydroxide (GFH), Water Res. 43 (2009) 490–498.
[9] Z. Amor, B. Bariou, N. Mameri, M. Taky, S. Nicolas, A. Elmidaoui, Fluoride removal from brackish water by electrodialysis, Desalination 133 (2001) 215–223.
[10] I. Abe, S. Iwasaki, T. Tokimoto, N. Kawasaki, T. Nakamura, S. Tanada, Adsorption of fluoride ions onto carbonaceous materials, J. Colloid Interface Sci. 275 (2004) 35–39.
[11] S.M. Maliyekkal, A.K. Sharma, L. Philip, Manganese-oxide-coated alumina: A promising sorbent for defluoridation of water, Water Res. 40 (2006) 3497–3506.
[12] S. Meenakshi, C.S. Sundaram, R. Sukumar, Enhanced fluoride sorption by mechanochemically activated kaolinites, J. Hazard. Mater. 153 (2008) 164–172.
[13] D. Mohan, K.P. Singh, V.K. Singh, Wastewater treatment using low cost activated carbons derived from agricultural byproducts—A case study, J. Hazard. Mater. 152 (2008) 1045–1053.
[14] A.L. López Valdivieso, J.L.R. Reyes Bahena, S. Song, R.H. Herrera Urbina, Temperature effect on the zeta potential and fluoride adsorption at the α-Al_2O_3/aqueous solution interface, J. Colloid Interface Sci. 298 (2006) 1–5.
[15] X. Wu, Y. Zhang, X.M. Dou, M. Yang, Fluoride removal performance of a novel Fe–Al–Ce trimetal oxide adsorbent, Chemosphere 69 (2007) 758–764.
[16] B.K. Biswas, J. Inoue, K. Inoue, K.N. Ghimire, H. Harada, K. Ohto, H. Kawakita, Adsorptive removal of As (V) and As(III) from water by a Zr(IV)-loaded orange waste gel, J. Hazard. Mater. 154 (2008) 1066–1074.
[17] G.K. Zhang, Z.L. He, W. Xu, A low-cost and high efficient zirconium-modified-Na-attapulgite adsorbent for fluoride removal from aqueous solutions, Chem. Eng. J. 183 (2012) 315–324.
[18] T. Yokoyama, Removal of fluoride anion by a porous spherical resin loaded with hydrous zirconium oxide, Chem. Lett. 18 (1989) 1155–1158.
[19] X.P. Liao, B. Shi, Adsorption of fluoride on zirconium (IV)-impregnated collagen fiber, Environ. Sci. Technol. 39 (2005) 4628–4632.
[20] S.K. Swain, S. Mishra, T. Patnaik, R.K. Patel, U. Jha, R.K. Dey, Fluoride removal performance of a new

hybrid sorbent of Zr(IV)–ethylenediamine, Chem. Eng. J. 184 (2012) 72–81.
[21] G. Alagumuthu, M. Rajan, Equilibrium and kinetics of adsorption of fluoride onto zirconium impregnated cashew nut shell carbon, Chem. Eng. J. 158 (2010) 451–457.
[22] R. Leyva-Ramos, J. Rivera-Utrilla, N.A. Medellin-Castillo, M. Sanchez-Polo, Kinetic modeling of fluoride adsorption from aqueous solution onto bone char, Chem. Eng. J. 158 (2010) 458–467.
[23] C. Janardhana, G.N. Rao, R.S. Sathish, P.S. Kumar, V.A. Kumar, M.V. Madhav, Study on defluoridation of drinking water using zirconium ion impregnated activated charcoals, Indian J. Chem. Technol. 14 (2007) 350–354.
[24] S.K. Swain, T. Patnaik, V.K. Singh, U. Jha, R.K. Patel, R.K. Dey, Kinetics, equilibrium and thermodynamic aspects of removal of fluoride from drinking water using meso-structured zirconium phosphate, Chem. Eng. J. 171 (2011) 1218–1226.
[25] N. Das, P. Pattanaik, R. Das, Defluoridation of drinking water using activated titanium rich bauxite, J. Colloid Interface Sci. 292 (2005) 1–10.
[26] S.S.Tripathy, S.B.Kanungo, Adsorption of Co^{2+}, Ni^{2+}, Cu^{2+} and Zn^{2+} from 0.5 M NaCl and major ion sea water on a mixture of δ-MnO_2 and amorphous FeOOH, J. Colloid Interface Sci., 284 (2005) 30–38.
[27] Y. Zhang, M. Yang, X. Huang, Arsenic(V) removal with a Ce(IV)-doped iron oxide adsorbent, Chemosphere 51 (2003) 945–952.
[28] R. Leyva Ramos, J. Ovalle-Turrubiartes, M.A. Sanchez-Castillo, Adsorption of fluoride from aqueous solution on aluminum-impregnated carbon, Carbon 37 (1999) 609–617.
[29] A.M. Raichur, M.J. Jyoti Basu, Adsorption of fluoride onto mixed rare earth oxides, Sep. Purif. Technol. 24 (2001) 121–127.
[30] E. Tchomgui-Kamga, V. Alonzo, C.P. Nanseu-Njiki, N. Audebrand, E. Ngameni, A. Darchen, Preparation and characterization of charcoals that contain dispersed aluminum oxide as adsorbents for removal of fluoride from drinking water, Carbon 48 (2010) 333–343.
[31] N.I. Chubar, V.A. Kanibolotskyy, V.V. Strelko, G.G. Gallios, V.F. Samanidou, T.O. Shaposhnikova, V.G. Milgrandt, I.Z. Zhuravlev, Adsorption of phosphate ions on novel inorganic ion exchangers, Colloids Surf., A 255 (2005) 55.
[32] Y.M. Zheng, S.F. Lim, J.P. Chen, Preparation and characterization of zirconium-based magnetic sorbent for arsenate removal, J. Colloid Interface Sci. 338 (2009) 22–29.
[33] A. Eskandarpour, M.S. Onyango, A. Ochieng, S. Asai, Removal of fluoride ions from aqueous solution at low pH using schwertmannite, J. Hazard. Mater. 152 (2008) 571–579.
[34] S. Figaro, J.P. Avril, F. Brouers, A. Ouensanga, S. Gaspard, Adsorption studies of molasse's wastewaters on activated carbon: Modelling with a new fractal kinetic equation and evaluation of kinetic models, J. Colloid Interface Sci. 161 (2009) 649–656.
[35] Y.S. Ho, G. Mckay, The kinetics of sorption of divalent metal ions onto sphagnum moss peat, Water Res. 34 (2000) 735–742.
[36] B. Kemer, D. Ozdes, A. Gundogdu, V.N. Bulut, C. Duran, M. Soylak, Removal of fluoride ions from aqueous solution by waste mud, J. Hazard. Mater. 168 (2009) 888–894.
[37] S. Kagne, S. Jagtap, P. Dhawade, S.P. Kamble, S. Devotta, S.S. Rayalu, Hydrated cement: A promising adsorbent for the removal of fluoride from aqueous solution, J. Colloid Interface Sci. 154 (2008) 88–95.
[38] H. Liu, S.B. Deng, Z.J. Li, G. Yu, J. Huang, Preparation of Al–Ce hybrid adsorbent and its application for defluoridation of drinking water, J. Hazard. Mater. 179 (2010) 424–430.
[39] K. Biswas, S.K. Saha, U.C. Ghosh, Adsorption of fluoride from aqueous solution by a synthetic iron (III)-aluminum(III) mixed oxide, Ind. Eng. Chem. Res. 46 (2007) 5346–5356.
[40] K. Babaeivelni, A.P. Khodadoust, Adsorption of fluoride onto crystalline titanium dioxide: Effect of pH, ionic strength, and co-existing ions, J. Colloid Interface Sci. 394 (2013) 419–427.
[41] N. Viswanathan, S.M. Prabhu, S. Meenakshi, Development of amine functionalized co-polymeric resins for selective fluoride sorption, J. Fluorine Chem. 153 (2013) 143–150.
[42] S.K. Swain, T. Patnaik, P.C. Patnaik, U. Jha, R.K. Dey, Development of new alginate entrapped Fe(III)–Zr(IV) binary mixed oxide for removal of fluoride from water bodies, Chem. Eng. J. 215–216 (2013) 763–771.
[43] L.Y. Chai, Y.Y. Wang, N. Zhao, W.C. Yang, X.Y. You, Sulfate-doped Fe_3O_4/Al_2O_3 nanoparticles as a novel adsorbent for fluoride removal from drinking water, Water Res. 47 (2013) 4040–4049.
[44] R.H. Huang, B.C. Yang, Q. Liu, K.L. Ding, Removal of fluoride ions from aqueous solutions using protonated cross-linked chitosan particles, J. Fluorine Chem. 141 (2012) 29–34.
[45] B.J. Liu, D.F. Wang, G.L. Yu, X.H. Meng, Removal of F^- from aqueous solution using Zr(IV) impregnated dithiocarbamate modified chitosan beads, Chem. Eng. J. 228 (2013) 224–231.
[46] X.M. Dou, D. Mohan, Charles U. Pittman, Remediating fluoride from water using hydrous zirconium oxide, Chem. Eng. J. 198–199 (2012) 236–245.
[47] G.C. Lv, L.M. Wu, L.B. Liao, Y.H. Zhang, Z.H. Li, Preparation and characterization of red mud sintered porous materials for water defluoridation, Appl. Clay Sci. 74 (2013) 95–101.
[48] V. Tomar, S. Prasad, D. Kumar, Adsorptive removal of fluoride from water samples using Zr–Mn composite material, Microchem. J. 111 (2013) 116–124.